Applied Thermal Engineering 132 (2018) 30–37

Contents lists available at ScienceDirect

Applied Thermal Engineering

journal homepage: www.elsevier.com/locate/apthermeng

Research Paper

Natural convection in a cross-fin heat sink

Shangsheng Feng [a], Meng Shi [b], Hongbin Yan [c], Shanyouming Sun [a], Feichen Li [a], Tian Jian Lu [a,*]

[a] State Key Laboratory for Strength and Vibration of Mechanical Structure, MOE Key Laboratory for Multifunctional Materials and Structures (LMMS), Shaanxi Engineering Laboratory for Vibration Control of Aerospace Structures, School of Aerospace, Xi'an Jiaotong University, Xi'an 710049, PR China
[b] School of Energy and Power Engineering, Xi'an Jiaotong University, Xi'an 710049, PR China
[c] School of Marine Science and Technology, Northwestern Polytechnical University, Xi'an 710072, PR China

HIGHLIGHTS

- A novel cross-fin heat sink was proposed for electronics cooling.
- Natural convection of the heat sink was experimentally and numerically examined.
- The overall heat transfer was enhanced by 11% than the plate-fin heat sink.
- Importantly, the geometrical complexity and material consumption was not increased.

ARTICLE INFO

Article history:
Received 4 July 2017
Revised 9 October 2017
Accepted 10 December 2017
Available online 11 December 2017

Keywords:
Plate-fin heat sink
Cross-fin heat sink
Natural convection
Heat transfer enhancement

ABSTRACT

A novel cross-fin heat sink consisting of a series of long fins and a series of perpendicularly arranged short fins was proposed to enhance natural convective heat transfer. The design principle of the cross-fin heat sink was based on overcoming internal thermal fluid-flow defects in a conventional plate-fin heat sink. The thermal performance of the proposed heat sink was compared with a reference plate-fin heat sink in horizontal orientation. A numerical model considering both natural convection and radiation heat transfer was developed to obtain thermal fluid-flow distributions and heat transfer coefficients of both the cross- and plate-fin heat sinks. Corresponding experiments were performed to validate the model predictions. It was demonstrated that, compared to the reference plate-fin heat sink, the cross-fin heat sink enhanced the overall (including natural convection and radiation) and convective (excluding radiation) heat transfer coefficients by 11% and 15%, respectively. Importantly, the enhancement was achieved without increasing the overall volume, material consumption, and too much extra cost. The proposed cross-fin heat sink provides a practical alternative to the widely adopted plate-fin heat sinks.

© 2017 Elsevier Ltd. All rights reserved.

1. Introduction

The longevity, performance and reliability of electronic components decay sharply as the operational temperature is increased, and hence it is crucial to include appropriate thermal management solutions in the electronic devices. To this end, broadly speaking, two thermal management solutions can be adopted: active cooling and passive cooling. Active cooling is usually realized by forcing the coolant to pass through an electronic component to take away the exhaust heat, whereas passive cooling utilizes natural convection and radiation heat transfer to dissipate the exhaust heat to ambient. Although active cooling yields a higher heat transfer rate, it requires an additional pump or fan to drive the coolant flow, causing extra energy consumption and noise. In contrast, passive cooling is devoid of these issues and more reliable since no moving parts are involved.

The performance of passive cooling is usually enhanced by using heat sinks. Plate-fin heat sink is one of the most widely accepted heat sinks for its simple geometry and low cost. The thermal characteristics and parameter optimization of plate-fin heat sinks have been extensively investigated. Bar-Cohen [1] found that a maximizing value of fin thickness existed for each distinct combination of environmental, geometric and material constraints. Jones and Smith [2] experimentally investigated plate-fins on horizontal surfaces and obtained optimal fin spacing as a function of fin height and temperature difference at a given fin length. Optimization of horizontal fin arrays was also conducted by Baskaya et al. [3] using a finite volume model. Bar-Cohen et al. [4] developed a least-material optimization procedure for vertical

* Corresponding author.
E-mail address: tjlu@mail.xjtu.edu.cn (T.J. Lu).

https://doi.org/10.1016/j.applthermaleng.2017.12.049
1359-4311/© 2017 Elsevier Ltd. All rights reserved.

Nomenclature

A_{sub}	base area of substrate (m^2)	Q_{rad}	radiative heat transfer rate (W)
h_{ovl}	overall heat transfer coefficient (W/m^2 K)	Q_{con}	convective heat transfer rate (W)
h_{con}	convective heat transfer coefficient (W/m^2 K)	ΔT	temperature difference (K)

plate-fin arrays in natural convective heat transfer. Optimized vertical plate-fin array parameters as functions of dimensions, thermal conductivity, emissivity, and fluid properties were numerically examined by Lieto Vollaro et al. [5]. Recently, Shen et al. [6] carried out an experimental and numerical study of the orientation effects on natural convective heat transfer in plate-fin heat sinks, and proposed correlations in a simple form $Nu = CRa^m$ for various orientations and Rayleigh numbers. Tari and coauthors [7–9] systematically examined the effects of orientation, length, height, and fin spacing on natural convective heat transfer of pate-fin heat sinks and proposed comprehensive correlations covering a wide range of parameters. Considering the fact that heat sinks were usually placed in shrouded enclosures in electronics, Naik et al. [10] firstly experimentally investigated the natural convective cooling of plate-fin heat sinks placed horizontally beneath an adiabatic shroud. They showed that lower optimal fin spacing and higher heat transfer rate ensued when the shroud clearance to the fin height ratio increased from zero to unity. Later, Yalcin et al. [11] performed a numerical analysis on the natural convection heat transfer from horizontal plate-fin heat sinks in the presence of a top shroud. Different geometrical parameters such as fin height, fin length, fin spacing, and top clearance were varied in a wide range of parameters. The results revealed the optimum fin spacing and showed that the average heat transfer coefficient increased with the increase in the value of the clearance parameter. Dogan and Sivrioglu [12] experimentally investigated the mixed convection heat transfer from plate-fin heat sinks inside a horizontal channel in the natural convection dominated region. Their results of experiments have shown that to obtain maximum amount of heat transfer in natural convection dominated region, the fin spacing should be at an optimum value about 8–12 mm within the range of parameters covered in the study.

Besides the widely used plate-fin heat sinks, various fin modifications have been proposed to enhance natural convective heat transfer, such as plate-fins with non-rectangular cross-sections [13], sloped plate-fins [14], radial plate-fin arrays [15–19], perforated pin-fins [20], and metal foams [21–23]. Kim et al. [13] investigated the natural convective heat transfer performance of vertical plate-fins with various cross-sections. Heat sinks with sloped plate-fins was proposed for natural convective heat transfer enhancement by Ledezma and Bejan [14]. Lee et al. [15] optimized a radial heat sink with respect to its fin-height profile to simultaneously minimize the thermal resistance and mass using a multi-disciplinary optimization. Upon matching relevant variables (number of fins, fin height, fin length and fin thickness) of a radial plate-fin heat sink, Costa and Lopes [16] presented an improvement procedure to obtain specific cooling effect with minimal usage of material mass. Jang et al. [17] examined the orientation effects of a radial plate-fin heat sink in natural convection and radiation. Further heat transfer enhancement of radial plate-fin heat sinks was demonstrated by incorporating a chimney with the heat sink [18,19]. Elshafei [20] proposed a heat sink with hollow/perforated circular pin fins and found that its natural convective heat transfer performance was better than that with solid pins.

Although numerous heat sink types have been proposed in the past decades, plate-fin heat sinks are still the mainstream due to good thermal performance and simple geometry. Therefore, a practical heat sink requires not only superior performance but also a simple geometry and low manufacture cost. In this study, a novel cross-fin heat sink was proposed for natural convective heat transfer enhancement with a rather simple geometry. A comparative case study was performed between the proposed cross-fin heat sink and the plate-fin heat sink. Numerical simulations were carried out considering both natural convection and radiation, and validated by heat transfer experiments. Thermal fluid-flow distributions, convective and overall heat transfer coefficients of the two heat sinks were comparatively analyzed to demonstrate the advantages of the proposed heat sink. This study showed one may improve the design of heat sink by exploring the internal thermal fluid-flow defects in a conventional plate-fin heat sink.

2. Heat sink design

The study was initiated from an industrial project aiming to design a heat sink for thermal management of indoor small cells for communication. In this scenario, the device was hung from a ceiling and there was a gap of 20 mm between the fin tip and the ceiling, as shown in Fig. 1. The objective was to reduce the temperature rise on the substrate of heat sink by 3–5 °C on top of a reference plate-fin heat sink for a given heat dissipation rate of 40 W. The dimensions of the reference plate-fin heat sink are shown in Fig. 2(a). Overall dimensions of the heat sinks were 200 × 200 × 21 mm^3 (length × width × height), with a height of 3 mm for the substrate and 18 mm for the fins. The thickness of each fin was 2 mm. The number of the plate-fins were claimed to be optimized in engineering conditions by the manufacturer, yielding an inter fin spacing of 10.38 mm, which was close to the optimal fin spacing reported in Ref. [11].

Fig. 2(b) shows geometrical notations of the proposed cross-fin heat sink, which included a series of parallel long fins as well as short fins perpendicularly arranged with respect to the long fins. The design philosophy of the cross-fin heat sink will be explained in Section 4. The long fins in the cross-fin heat sink had the same length as the reference plate-fin heat sink (200 mm), while the length of the short fins in the cross-fin heat sink was 50 mm. The parameters of the plate- and cross-fin heat sinks were summarized in Table 1. As shown in the Table 1, the overall volume, material mass, as well as heat transfer surface area of the two heat sinks were essentially identical.

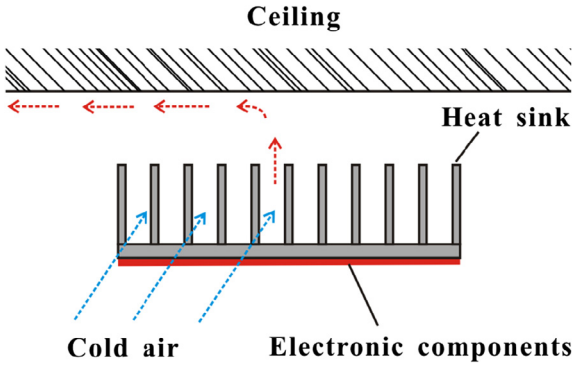

Fig. 1. Schematic of a heat sink placed beneath the ceiling with a gap between the heat sink and ceiling.

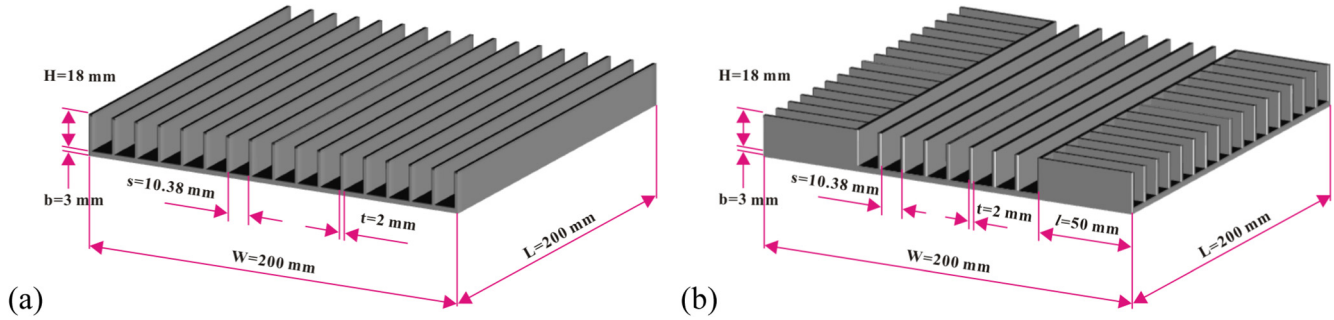

Fig. 2. Schematic of (a) conventional plate-fin heat sink and (b) proposed cross-fin heat sink.

3. Methods

3.1. Experiment

Experiments were conducted to verify the design of the proposed heat sink as well as validate the numerical model detailed in the next subsection. A plate-fin heat sink (as reference) and a cross-fin heat sink were cut out from aluminum blocks with parameters depicted in Fig. 2. Pictures of the two fabricated heat sinks were displayed in Fig. 3(a) and (b).

Fig. 3(c) shows the test setup of natural convection experiment. In order to house thermocouples, three slots were cut from the lower surface of the substrate of each heat sink with a cross-sectional area of 1×1 mm^2. Nine 36-gauge T-type bead thermocouples (Omega, wire diameter: 0.127 mm) were embedded in the slots to measure the average temperature of the substrate. The remaining gaps of the three slots were then filled with thermal grease to ensure the lower surface of the substrate was flat. The substrate of heat sink was virtually divided into 4×4 control volumes, and thermocouples were located at the center of the control volumes. The layout of the thermocouples on the substrate was depicted in Fig. 4(a). Due to symmetry, only one quarter of the substrate region was monitored to obtain the average temperature of the substrate. The high thermal conductivity of aluminum resulted in uniform temperature distribution in the substrate.

A film heating pad was subsequently attached to the substrate of heat sink to apply uniform heating. The film heating pad having a total thickness of 0.3 mm was made of etched foil insulated with kapton material, as shown in Fig. 4(b). The heat sink with heating pad was placed onto a 45 mm thick thermal insulation foam (polyurethane, $k \sim 0.036$ W/mK) to ensure the majority of the imposed heat was conducted to the heat sink. The heat sink with heating and thermal insulation assembly was then positioned horizontally on a flat plate (bottom plate) of 400 mm $\times$ 400 $\times$ 10 mm in size, as shown in Fig. 3(c). A top plate made by Perspex of 400 mm $\times$ 400 mm $\times$ 10 mm in size was suspended 20 mm above the heat sink. The bottom and top plates were painted in black to identify the thermal radiation emissivity. A DC power supply (Agilent) was used to power the film heating pad. A temperature scanner (Agilent, 34970A) connected to a laptop was employed to receive signals from thermocouples (nine for temperature of heat sink, and another two for ambient temperature). To avoid the fluctuation of ambient temperature, all the test apparatus except the DC power supply and the data recording computer were placed in an enclosure of 1.5 m $\times$ 1.5 m $\times$ 2 m. More details on the experimental setup can be referred to Ref. [23].

3.2. Numerical simulation

Due to symmetry, the 1/4 of each heat sink was chosen as the computational domain to save computational time. The computational domain for the cross-fin heat sink was shown in Fig. 5, while that for the plate-fin heat sink was omitted for conciseness. To consider heat loss from the insulation foam, the insulation foam was included in the computational domain. Therefore, the entire computational domain included three subdomains, i.e., the insulation foam (indicated by yellow), the heat sink (with the substrate indicated by pink and the fins by grey), and the air. The origin of the Cartesian coordinates was placed at the bottom center of the substrate, as shown in Fig. 5.

For both heat sinks, natural convection and radiation heat transfer were considered. The flow was taken as three-dimensional, laminar and steady. Radiation heat transfer was modeled using the discrete ordinates model (DO model) which supported the symmetry boundary condition. Relevant governing equations were summarized as below.

Continuity equation:

$$\nabla \cdot (\rho \mathbf{v}) = 0 \tag{1}$$

Momentum equation:

$$\rho \frac{D\mathbf{v}}{Dt} = -\nabla p + \eta \nabla^2 \mathbf{v} + \mathbf{F} \quad (\text{for z-direction } \mathbf{F}_z = -\rho g) \tag{2}$$

Energy equation:

$$\rho c_p \frac{DT}{Dt} = \nabla \cdot (\lambda \nabla T) + S_h \tag{3}$$

Radiative transfer equation (DO model):

$$\nabla \cdot (I(\vec{r}, \vec{s})\,\vec{s}) + (a + \sigma_s) I(\vec{r}, \vec{s}) = an^2 \frac{\sigma T^4}{\pi} + \frac{\sigma_s}{4\pi} \int_0^{4\pi} I(\vec{r}, \vec{s}')\Phi(\vec{s} \cdot \vec{s}')d\Omega' \tag{4}$$

Solid region energy equation:

$$\nabla \cdot (\lambda \nabla T) + S_h = 0 \tag{5}$$

Table 1
Parameters of the plate- and cross-fin heat sinks.

Heat sink	Overall volume (mm $\times$ mm $\times$ mm)	Mass (kg)	Surface area density (m^2/m^3)	Fin thickness (mm)	Fin height (mm)	Fin spacing (mm)
Plate-fin	200 $\times$ 200 $\times$ 21	0.656	1977	2	18	10.38
Cross-fin	200 $\times$ 200 $\times$ 21	0.664	2005	2	18	10.38

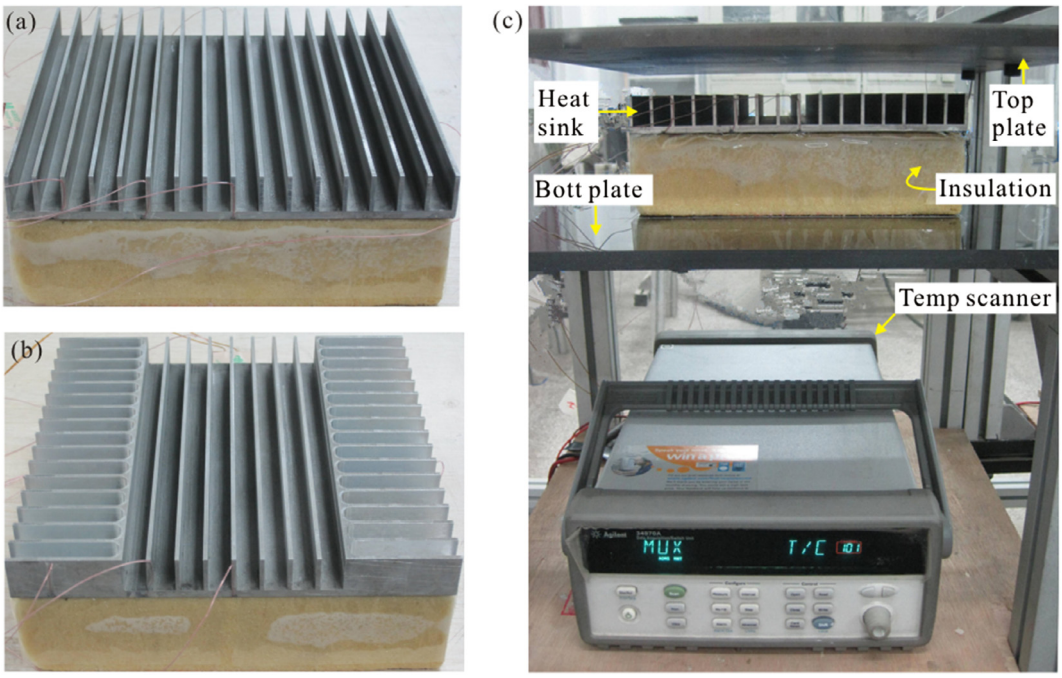

Fig. 3. Test samples and experimental setup: (a) conventional plate-fin heat sink; (b) cross-fin heat sink; (c) experimental setup.

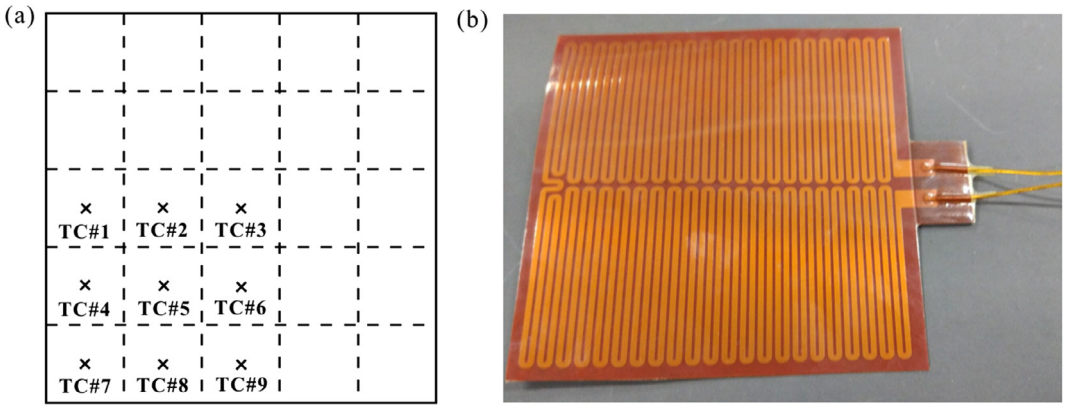

Fig. 4. (a) Layout of thermocouples on substrate and (b) the film heating pad.

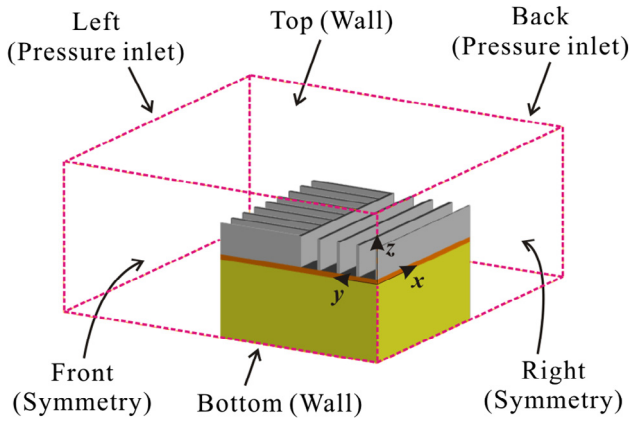

Fig. 5. Computational domain and boundary conditions for cross-fin heat sink.

Eqs. (1)–(3) were applied for natural convection of air in the computational domain, where ρ, c_p, η,and λ were density, specific heat, viscosity, and thermal conductivity of air, respectively. These thermal properties were all modeled as functions of temperature except that the specific heat was hold constant. S_h in Eq. (3) represented the radiation source term, and the coupling strategy between the energy equation and the radiation equation was referred to [24].

Eq. (4) was for radiation heat transfer, where I was the radiation intensity which depended on the position vector $(\vec{r})$ and direction vector $(\vec{s})$. σ was the Stefan-Boltzmann constant. a, σ_s, and n were separately the absorption coefficient, scattering coefficient, and refractive index of each heat transfer medium. Since air is transparent to thermal radiation, the three parameters of air were set to be 0, 0, and 1, respectively. The insulation foam and the heat sink were assumed to be opaque (i.e., optically thick) so that thermal radiation could not transmit through, which means that radiation energy was transmitted into thermal energy on the surfaces of the insulation foam and heat sink. The values of a, σ_s and n for

the insulation foam and heat sink should therefore not influence the computational results under the opaque medium assumption. Further, all the radiation surfaces were assumed to be gray and diffuse. The emissivity on heat sink surfaces was characterized to be 0.32, which was identical to the radiation property of oxidized aluminum [25]. The emissivity on all other radiation surfaces was set to be unit.

Heat conduction in the insulation foam and heat sink was described with Eq. (5). The thermal conductivity of aluminum (heat sink) and polyurethane (insulation foam) was specified to be 202 W/mK and 0.036 W/mK, respectively. S_h in Eq. (5) was the volumetric heat source applied for the heat sink substrate.

Fig. 5 displays the boundary conditions applied in the simulation. Symmetry boundary condition was applied at the front and right surfaces of the computational domain. Pressure inlet boundary condition was prescribed at the left and back surfaces. Non-slip wall boundary condition was imposed at both the top and bottom surfaces. The bottom surface was assumed to be adiabatic. To ensure the accuracy of simulation, the top surface of the computational domain was treated as a "conducting wall" in Fluent, with the wall thickness and thermal conductivity specified to be 10 mm and 0.2 W/mK, respectively. In order to simulate heat loss from the top surface to the ambient, a mixed thermal boundary condition (natural convection and radiation) was applied at the top surface with the natural convective heat transfer coefficient assumed to be 5 W/m^2 K and the external radiation emissivity to be unit.

A commercial CFD code (ANSYS Fluent 14.5) was used to solve the current problem as formulated. The SIMPLE algorithm was applied to couple the pressure and velocity for numerical analysis. To enhance the accuracy of the calculation results, a second-order upwind scheme was applied to discretize the convective terms of governing equations [26,27]. The iterative convergence criterion was chosen as 10^{-4} for momentum equation and 10^{-6} for energy equation. Structured mesh was generated in Gambit with grids refined near wall surfaces. To check the grid dependency, the first grid distance from the wall was varied from 0.2 mm to 0.4 mm, yielding a total grid number of 820,000 and 528,000 for the plate-fin heat sink. Numerical results obtained from the two grids were found to have a discrepancy less than 1%.

4. Results and discussion

Natural convection and radiation heat transfer of cross-fin heat sink and its counterpart plate-fin heat sink was simulated with varying heat inputs from 20 to 60 W. A heat input over 60 W resulted in the chip temperature higher than 100 °C for the heat sinks investigated in the study, which was not practical and should be avoided. Thermal fluid-flow distributions in the two heat sinks were analyzed to explore the merits of the cross-fin heat sink. Overall and convective heat transfer coefficients of the two heat sinks were compared. For validation, numerical simulation results were compared with experiment measurements.

Firstly, thermal fluid-flow in plate-fin heat sink is examined. Fig. 6(a) presents the velocity field in a slice coinciding with the mid-width of a fin channel in the plate-fin heat sink, which shows the flow pattern of air entering and exiting the heat sink. Note that only 1/4 of the heat sink is shown and the *x*-*z* and *y*-*z* planes are symmetrical planes. As shown in Fig. 6(a), a large amount of air entering the heat sink is from the vertically rising flow along the insulation foam (not shown in the figure) beneath the heat sink. At the fin channel entrance, this vertically rising flow changes its direction to horizontal since the vertical flow is suppressed by the horizontal inlet flow at the top of the channel entrance. The entering flow velocity is maximized near the channel entrance, and decays gradually as the flow moves towards the channel center. The exiting flow forms a boundary layer near the top wall. The flow rate of the exiting flow increases from the channel center to the entrance, reflecting that only a limited amount of air could reach the channel center.

Fig. 6(b) presents the temperature distribution in a slice coinciding with the mid-width of a fin channel in the plate-fin heat sink. The results show that cold fresh air can only penetrate into the channel over a certain distance from the entrance, which coincides with the velocity distribution in Fig. 6(a), while the high temperature region near the channel center implies inefficient heat transfer in the region. In summary, the present results of velocity and temperature distributions point to a major deficiency of the conventional plate-fin heat sink, that is, it is difficult for cold flow to reach the center of fin channels.

In order to overcome (at least partially) the deficiency of the plate-fins, in the cross-fin heat sink, the fins were split into a series of long fins and another series of short fins, as shown in Fig. 2(b). The velocity and temperature distributions in a slice coinciding with the mid-width of a long fin channel in the cross-fin heat sink are shown in Fig. 7(a) and (b), respectively. Corresponding results for a short fin channel are presented in Fig. 7(c) and (d), respectively. As shown in Fig. 7(a) and (b), the velocity and temperature distributions in the long channel of cross-fin heat sink are similar to those in plate-fin heat sink. However, surprisingly, for the short fins as shown in Fig. 7(c) and (d), the fresh air is able to invade the entire fin channel, thereby yielding a higher average heat transfer rate on the short fins than on the long fins. Further, as shown in Fig. 7(c), the flow entering the short fin channel eventually impinges toward the endwall of the channel, i.e., the long fin that intersects with the short fins. The impingement flow should cause a higher local heat transfer rate than parallel flow [28], thus

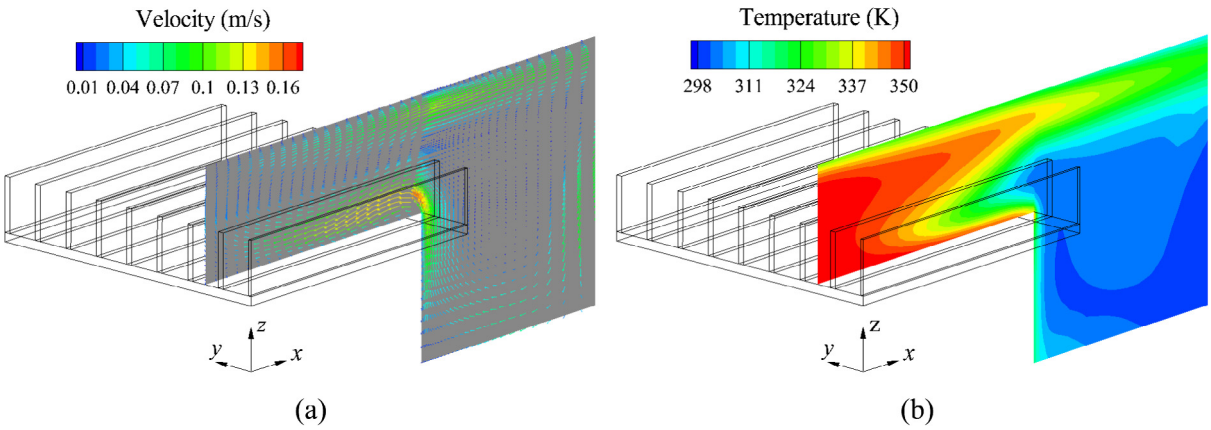

Fig. 6. Thermal and fluid-flow distributions in plate-fin heat sink: (a) velocity field in a fin channel; (b) temperature field in the same fin channel.

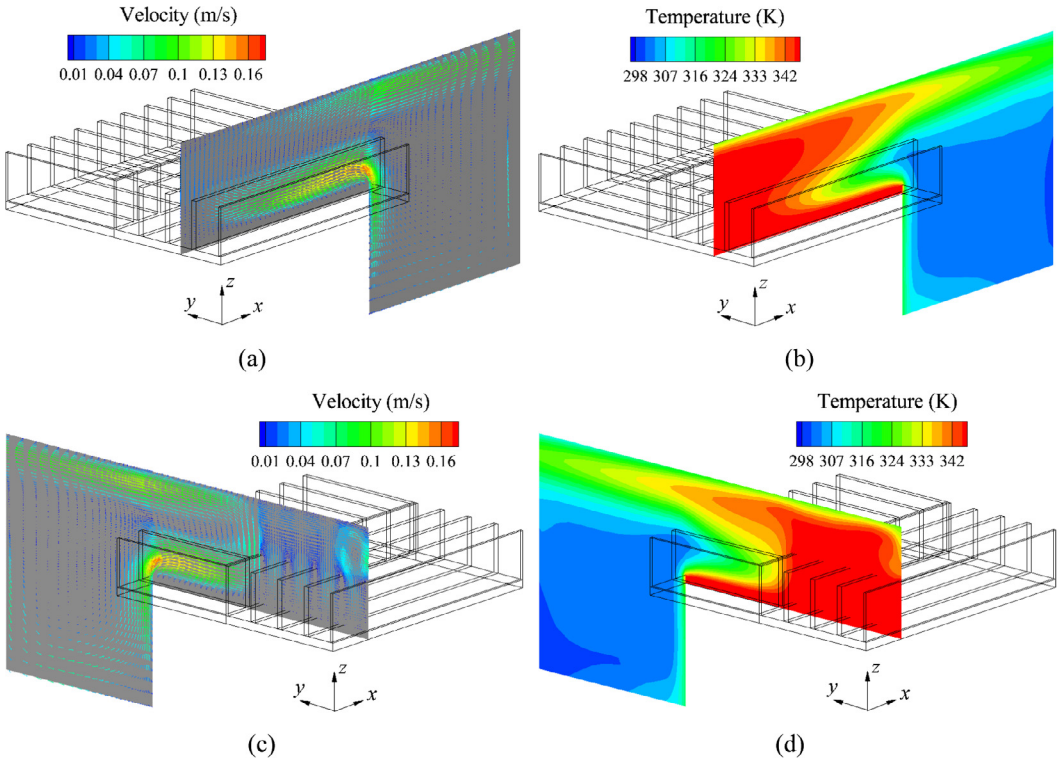

Fig. 7. Thermal and fluid-flow distributions in cross-fin heat sink: (a) velocity field in a long fin channel; (b) temperature field in the same long fin channel; (c) velocity field in a short fin channel; (d) temperature field in the same short fin channel.

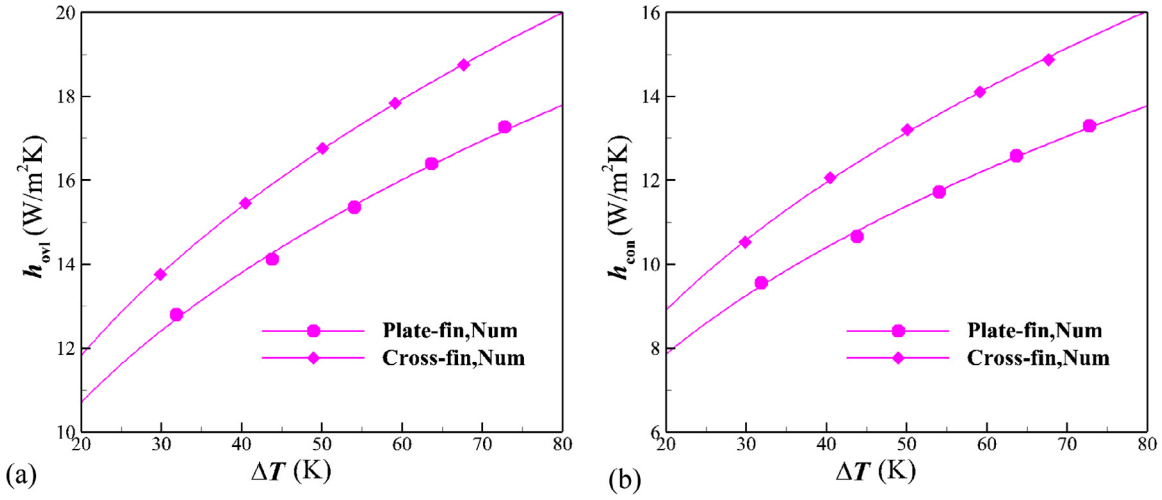

Fig. 8. Thermal performance comparison between plate- and cross-fin heat sinks: (a) overall heat transfer coefficient considering both convection and radiation; (b) convective heat transfer coefficent.

providing another advantage of the cross-fin heat sink for heat transfer enhancement.

To facilitate quantitative comparison between the two heat sinks, the overall and convective heat transfer coefficients are defined as:

$$h_{ovl} = \frac{Q_{rad} + Q_{con}}{A_{sub}\Delta T} \tag{6}$$

$$h_{con} = \frac{Q_{con}}{A_{sub}\Delta T} \tag{7}$$

where Q_{rad} and Q_{con} are separately the radiative and convective heat transfer rate from the heat sink; A_{sub} is the base area of the heat sink substrate; and ΔT is the temperature difference between the substrate and the ambient. The overall heat transfer coefficient includes both convective and radiative contributions, while the convective heat transfer coefficient considers only convective contribution.

Fig. 8(a) and (b) compare the overall and convective heat transfer coefficients of the proposed cross-fin heat sink with those of the conventional plate-fin heat sink, respectively. The overall and convective heat transfer coefficients of the proposed heat sink are 11% and 15% higher than those of the conventional plate-fin heat sink, respectively. Radiation heat transfer in the two heat sinks is similar, and hence heat transfer enhancement due to cross-fins is contributed mainly by improved thermal fluid-flow within the heat sink.

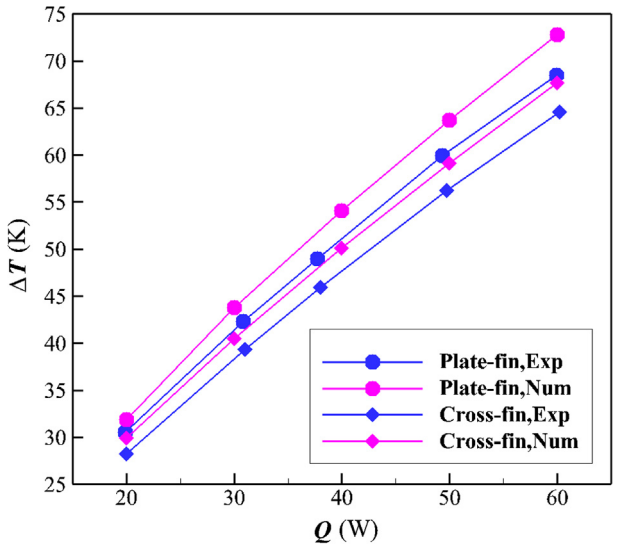

Fig. 9. Temperature rises of plate- and cross-fin heat sinks plotted as a function of heat input: experiment versus sumulation.

Importantly, the weight and overall volume of the cross-fin heat sink is almost identical as that of the reference plate-fin heat sink (see Table 1), therefore one does not need to sacrifice the compactness of heat sink for heat transfer enhancement. In addition, compared to other fin types for heat transfer enhancement, the cross-fin heat sink has quite simple geometry. In reality, one may assemble three plate-fin heat sinks together (one with long fins and the other two with short fins) to the form the cross-fin heat sink. In this case, cheap manufacture techniques such as aluminum extrusion can be used to produce the cross-fin heat sink. In this regard, the heat transfer improvement can be achieved without too much extra cost with the cross-fin heat sink. Furthermore, the thermal performance of the cross-fin heat sink may be further improved by optimizing its geometric parameters, such as length and fin spacing of the short fins. Due to superior thermal performance and simple geometry, the proposed cross-fin heat sink would be a practical alternative of conventional plate-fin heat sinks.

Finally, the experimental and numerical results are compared. Fig. 9 plots the experimentally and numerically obtained temperature rises on the substrates of the two heat sinks as a function of the heat inputs. In the figure, the symbol circle denotes the plate-fin heat sink, and the diamond represents the cross-fin heat sink. The color pink indicates the numerical results, and the blue stands for the experimental results. Both experimental and numerical results show that the temperature rises of the cross-fin heat sink are systematically lower than the plate-fin heat sink. The numerically simulated temperature rises are 6% and 5% higher than the experimental results for the plate- and cross-fin heat sinks, respectively. The higher temperature rises of numerical simulations may be caused by the adiabatic boundary condition applied at the bottom surface of the computational domain (see Fig. 5), which ignored heat loss from the bottom wall. In addition, uncertainties in the thermophysical properties (such as thermal conductivities of insulation foam and heat sink) and radiation emissivities used in the numerical model could also contribute deviations between experiment and simulation.

5. Conclusion

A novel cross-fin heat sink was proposed and demonstrated to improve natural convective heat transfer compared to a reference plate-fin heat sink widely used in electronics cooling. Numerical simulations considering both natural convection and radiation heat transfer were carried out, and validated by experimental measurements. For plate-fin heat sink, the simulation results showed that cold air only can penetrate a limited distance into the fin channel from heat sink entrance, thus causing inferior thermal efficiency at heat sink center. For cross-fin heat sink, the cold air was able to reach to the entire short fin channel and formed an impinging-like flow towards channel endwall, which was beneficial for heat transfer enhancement. Compared to plate-fin heat sink, the overall and convective heat transfer coefficients of cross-fin heat sink were increased by 11% and 15%, respectively. Such performance enhancement was mainly attributed to improved thermo-fluidic flow pattern in the cross-fin heat sink, as radiation contributions of the two heat sinks were similar. The concept of cross-fin opens a door to improve natural convective heat transfer in limited space without increasing material consumption and too much extra manufacture cost.

Acknowledgements

This work was supported by the National Key R&D Program of China (2016YFC0205600), the National Natural Science Foundation of China (51676156, 51206128), the National “111” Project of China (B06024), the Postdoctoral Science Foundation of China (2016M590942), the Shaanxi Province Science Foundation and the Fundamental Research Funds for the Central Universities of China.

References

[1] A. Bar-Cohen, Fin thickness for an optimized natural convection array of rectangular fins, J. Heat Transf. 101 (1979) 564–566.
[2] C.D. Jones, L.F. Smith, Optimum arrangement of rectangular fins on horizontal surfaces for free-convection heat transfer, J. Heat Transf. 92 (1970) 6–10.
[3] S. Baskaya, M. Sivrioglu, M. Ozek, Parametric study of natural convection heat transfer from horizontal rectangular fin arrays, Int. J. Therm. Sci. 39 (8) (2000) 797–805.
[4] A. Bar-Cohen, M. Iyengar, A.D. Kraus, Design of optimum plate-fin natural convective heat sinks, J. Electron. Packag. 125 (2003) 208–216.
[5] A. de Lieto Vollaro, S. Grignaffini, F. Gugliermetti, Optimum design of vertical rectangular fin arrays, Int. J. Therm. Sci. 38 (6) (1999) 525–529.
[6] Q. Shen, D. Sun, Y. Xu, T. Jin, X. Zhao, Orientation effects on natural convection heat dissipation of rectangular fin heat sinks mounted on LEDs, Int. J. Heat Mass Transf. 75 (2014) 462–469.
[7] Mehdi Mehrtash, Ilker Tari, A correlation for natural convection heat transfer from inclined plate-finned heat sinks, Appl. Therm. Eng. 51 (1) (2013) 1067–1075.
[8] Ilker Tari, Mehdi Mehrtash, Natural convection heat transfer from horizontal and slightly inclined plate-fin heat sinks, Appl. Therm. Eng. 61 (2) (2013) 728–736.
[9] Ilker Tari, Mehdi Mehrtash, Natural convection heat transfer from inclined plate-fin heat sinks, Int. J. Heat Mass Transf. 56 (1) (2013) 574–593.
[10] S. Naik, S.D. Probert, C.I. Wood, Natural-convection characteristics of a horizontally-based vertical rectangular fin-array in the presence of a shroud, Appl. Energy 28 (1987) 295–319.
[11] H.G. Yalcin, S. Baskaya, M. Sivrioglu, Numerical analysis of natural convection heat transfer from rectangular shrouded fin arrays on a horizontal surface, Int. Commun. Heat Mass Transf. 35 (2008) 299–311.
[12] M. Dogan, M. Sivrioglu, Experimental investigation of mixed convection heat transfer from longitudinal fins in a horizontal rectangular channel: In natural convection dominated flow regimes, Energy Convers. Manage. 50 (2009) 2513–2521.
[13] Dong-Kwon Kim, Thermal optimization of plate-fin heat sinks with fins of variable thickness under natural convection, Int. J. Heat Mass Transf. 55 (4) (2012) 752–761.
[14] Gustavo Ledezma, Adrian Bejan, Heat sinks with sloped plate fins in natural and forced convection, Int. J. Heat Mass Transf. 39 (9) (1996) 1773–1783.
[15] Daeseok Jang, Se-Jin Yook, Kwan-Soo Lee, Optimum design of a radial heat sink with a fin-height profile for high-power LED lighting applications, Appl. Energy 116 (2014) 260–268.
[16] Vítor A.F. Costa, António M.G. Lopes, Improved radial heat sink for led lamp cooling, Appl. Therm. Eng. 70 (1) (2014) 131–138.
[17] Daeseok Jang, Seung-Jae Park, Se-Jin Yook, Kwan-Soo Lee, The orientation effect for cylindrical heat sinks with application to LED light bulbs, Int. J. Heat Mass Transf. 71 (2014) 496–502.
[18] Bin Li, Young-Jin Baik, Chan Byon, Enhanced natural convection heat transfer of a chimney-based radial heat sink, Energy Convers. Manage. 108 (2016) 422–428.

[19] Seung-Jae Park, Daeseok Jang, Se-Jin Yook, Kwan-Soo Lee, Optimization of a chimney design for cooling efficiency of a radial heat sink in a LED downlight, Energy Convers. Manage. 114 (2016) 180–187.
[20] E.A.M. Elshafei, Natural convection heat transfer from a heat sink with hollow/perforated circular pin fins, Energy 35 (7) (2010) 2870–2877.
[21] A. Bhattacharya, R.L. Mahajan, Metal foam and finned metal foam heat sinks for electronics cooling in buoyancy-induced convection, J. Electron. Packag. 128 (3) (2006) 259–266.
[22] S.S. Feng, J.J. Kuang, T. Wen, T.J. Lu, K. Ichimiya, An experimental and numerical study of finned metal foam heat sinks under impinging air jet cooling, Int. J. Heat Mass Transf. 77 (2014) 1063–1074.
[23] S.S. Feng, F.C. Li, F.H. Zhang, T.J. Lu, Natural convection in metal foam heat sinks with open slots, Exp. Therm Fluid Sci. 91 (2018) 354–362.
[24] ANSYS FLUENT 14.5 User's & Tutorial Guide, ANSYS Inc., Canonsburg, PA, 2012.
[25] F.P. Incropera, D.P. DeWitt, T.L. Bergman, A.S. Lavine, Fundamentals of Heat and Mass Transfer, Wiley, 2007.
[26] G.L. Xu, X. Jiang, G. Liu, Delayed detached eddy simulations of fighter aircraft at high angle of attack, Acta Mech. Sin. 32 (4) (2016) 588–603.
[27] D.L. Guo, K.M. Shang, Y. Zhang, G.W. Yang, Z.X. Sun, Influences of affiliated components and train length on the train wind, Acta Mech. Sin. 32 (2) (2016) 191–205.
[28] K. Jambunathan, E. Lai, M.A. Moss, et al., A review of heat transfer data for single circular jet impingement, Int. J. Heat Fluid Flow 13 (2) (1992) 106–115.